Fluorescence Correlation Spectroscopy: The Case of Subdiffusion

Ariel Lubelski[†*] and Joseph Klafter[†‡]
[†]School of Chemistry, Raymond and Beverly Sackler Faculty of Exact Sciences, Tel Aviv University, Tel Aviv, Israel; and [‡]Institute for Advanced Studies (FRIAS), University of Freiburg, 79104, Freiburg, Germany

ABSTRACT The theory of fluorescence correlation spectroscopy is revisited here for the case of subdiffusing molecules. Subdiffusion is assumed to stem from a continuous-time random walk process with a fat-tailed distribution of waiting times and can therefore be formulated in terms of a fractional diffusion equation (FDE). The FDE plays the central role in developing the fluorescence correlation spectroscopy expressions, analogous to the role played by the simple diffusion equation for regular systems. Due to the nonstationary nature of the continuous-time random walk/FDE, some interesting properties emerge that are amenable to experimental verification and may help in discriminating among subdiffusion mechanisms. In particular, the current approach predicts 1), a strong dependence of correlation functions on the initial time (aging); 2), sensitivity of correlation functions to the averaging procedure, ensemble versus time averaging (ergodicity breaking); and 3), that the basic mean-squared displacement observable depends on how the mean is taken.

INTRODUCTION

The mobility of proteins in cell membranes has been of great interest, being essential for various biological functions on the cell level (1–4). Among various techniques (5–9) introduced to measure protein mobility, fluorescence correlation spectroscopy (FCS) (10,11), which measures time correlation functions of fluorescence fluctuations, has been quite widespread. This technique, which is a general technique for measuring mobility of molecules, is being used here for lateral motion. The fluorescence stems from tagged particles that move randomly on the membrane surface and perform mainly lateral diffusion. The random movement creates spontaneous local concentration changes that in turn cause fluorescence fluctuations.

In regularly behaving systems, the decay rate of concentration fluctuations is the same as the decay of a macroscopically perturbed system back to equilibrium. The decay of the macroscopic perturbations is described by the simple diffusion equation (12). There has been growing evidence, however, that protein diffusion might deviate from regular behavior. Several techniques, among them single particle tracking (SPT) (7,8), have demonstrated that in some cases, proteins display subdiffusion, characterized by a mean-squared displacement (MSD) that increases sublinearly rather than linearly with time (13,14). The origins of subdiffusion are yet to be determined. Some possible causes of subdiffusion have been suggested, for instance, interactions of proteins with the extracellular matrix or with other structures within and in proximity to membranes, or confinement due to geometrical obstacles, such as fences, created by the cytoskeleton.

There is clearly a need to revisit the theory of FCS to account for the possibility that protein movement is not always Brownian. Here, we calculate FCS curves assuming that continuous-time random walk (CTRW) (15) for subdiffusion (16,17) is applicable. The calculations follow the same path used in the case of regular diffusion (10) now modified to account for the anomalous behavior. The modification is based on the generalization of the diffusion equation to describe subdiffusion using fractional calculus (16,18).

In the framework of CTRW, the motion of particles is described by two decoupled probability density functions (PDFs), one for jump length and another for waiting time between jumps (16,18,19). The movement is then given by a sequence of jumps each followed by a waiting time. The jumps and waiting times are chosen from the corresponding PDFs. Each jump length and each waiting time are chosen independently, with no correlations. If the jump-length PDF and waiting-time PDF have second and first moments, respectively (variance and mean, respectively), the motion of particles will always yield normal diffusion.

Anomalous diffusion, aging, and ergodicity breaking

The regular behavior can be drastically modified by choosing waiting-time PDFs that do not have a well-defined mean. Such nonstationary PDFs are functions that decay slowly and are therefore asymptotically fat-tailed (16,20):

$$\Psi(t) \propto \frac{1}{\nu^{\alpha} t^{1+\alpha}},\ 0 < \alpha < 1,\ t >> 1/\nu, \qquad (1)$$

where $1/\nu$ is a characteristic time. Eq. 1 describes a situation in which there is a nonnegligible probability that a particle will get stuck in space for a very long time. The overall motion of particles that undergo diffusion with a waiting-time PDF (Eq. 1) is subdiffusive.

This anomalous behavior is usually defined by the MSD of the diffusing particles. Although for regular diffusion the MDS grows linearly with time,

Submitted March 14, 2008, and accepted for publication October 9, 2008.

*Correspondence: lubelski@post.tau.ac.il

Editor: Michael Edidin.

© 2009 by the biophysical society

0006-3495/09/03/2055/9 $2.00

doi: 10.1016/j.bpj.2008.10.069

$$\langle r^2(t)\rangle = 2dKt, \tag{2}$$

where d is the spatial dimension and K is the diffusion coefficient [$\frac{\text{length}^2}{\text{time}}$], in the anomalous case, the MSD follows (16)

$$\langle r^2(t)\rangle = \frac{2dK_\alpha}{\Gamma(1+\alpha)}t^\alpha \ , \ \alpha \neq 1, \tag{3}$$

where K_α is the anomalous diffusion coefficient of dimensions [length^2/time$^\alpha$], α is the anomaly exponent, and $\Gamma(x)$ is the gamma function (21). Here, we focus on subdiffusion so that $0 < \alpha < 1$. It should be mentioned that the averaging ($\langle\ \rangle$) in Eq. 3 stands for an ensemble average. We return to this delicate point below.

The fat-tailed PDF (Eq. 1) can stem from different origins that lead to subdiffusion. An example for such a mechanism is that of a system of local potential wells that act as momentary traps for particles, with the rate of leaving a trap given by (22)

$$b \propto \exp(-\Delta E/kT). \tag{4}$$

Here, ΔE is the activation energy needed to leave the trap. Assuming that the depths of the potential wells are distributed exponentially,

$$\rho(\Delta E) \propto \exp(-\Delta E/kT_0), \tag{5}$$

where $\rho\ (\Delta E)$ is the density of traps of depth ΔE and T_0 is an effective temperature that characterizes the trap distribution. In such systems, the waiting-time PDF follows a power law (22,23) as in Eq. 1, with

$$\alpha = T/T_0. \tag{6}$$

The motion is therefore subdiffusive for $T < T_0$, which corresponds to $0 < \alpha < 1$. For temperatures $T > T_0$ for which $1 < \alpha$, the waiting-time PDF possesses a first moment, and regular diffusion is expected (22).

Systems manifesting such anomalous behavior are characterized by aging and ergodicity breaking (24–27), which are an important concept when analyzing FCS data. Aging in CTRW systems with fat-tailed waiting-time PDFs (Eq. 1) means that as time evolves, fewer and fewer events occur per time interval (Fig. 1), demonstrating the growing probability that diffusing particles will get stuck for longer and longer times (28,29). The scenario that clarifies this effect is that of a system of particles each of which starts at time $t = 0$ by choosing a new waiting time from Eq. 1. Since the ''majority'' of waiting times will be small, most particles will, after the clock starts, be seen hopping around. Only a few will obtain a long waiting time. These particles will remain at their position for a long time. As time progresses, other particles will also ''get stuck,'' and by this effect one will begin to accumulate a growing fraction of particles that is not moving. This accumulation of ''stuck'' particles is the aging characteristic of systems manifesting this kind of anomalous subdiffusion. As a result, experimental observations depend on the time span of the measurement and on its starting time. Therefore, the initial conditions should be carefully dealt with. Here, we assume measurements that start at the same time that the system is prepared ($\tau = 0$). The starting time can be viewed from the CTRW point of view as the time when all particles start their random waiting period for the first jump. The aging characteristic is related to the nonstationary behavior (26,27) of the CTRW-type anomalous subdiffusion. That is to say, systems displaying such anomaly behave differently at different times. For example, the ensemble average of a concentration fluctuation is given (for the anomalous case with exponent α) by

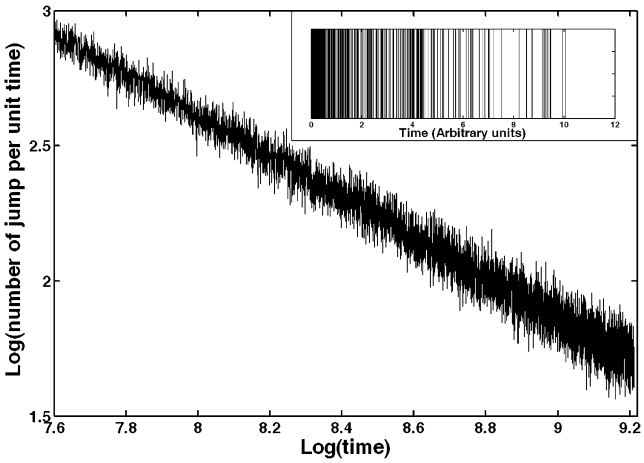

FIGURE 1 A log-log plot of the number of jumps (steps) in a time interval of one unit time (arbitrary units) as a function of time (for long times). The slope we obtain is for α 0.25: slop = α -1 = -0.75. (*Inset*) CTRW with 100 independent particles was simulated and the number of jumps was detected for the same time interval at different times. A fat-tailed waiting-time PDF was used with $\alpha = 0.25$. The decrease in the density of lines for larger times demonstrates the decrease in the number of events as time progresses and, thus, the aging concept.

$$B_\alpha^E(0,t) = \langle \delta C_\alpha(r,0)\delta C_\alpha(r,t)\rangle, \tag{7}$$

where $\delta C_\alpha\ (r,0)$ and $\delta C_\alpha\ (r,t)$ are the concentration fluctuations at location r at times 0 and t, respectively. The superscript E stands for an ensemble average over many systems. $B_\alpha^E(0,t)$ measures the concentration fluctuation at two precise times: 0 and t. However, contrary to a regular system, this ensemble average is different for the same time difference, t, as in Eq. 7, but relative to a different starting time, $\tau > 0$:

$$B_\alpha^E(\tau,t) = \langle \delta C_\alpha(r,\tau)\delta C_\alpha(r,\tau+t)\rangle. \tag{8}$$

Due to aging, as time evolves, the rate of steps decreases and $B_\alpha^E(\tau,t)$ decays more slowly compared to $B_\alpha^E(0,t)$, and therefore, these two averages yield different behaviors, $B_\alpha^E(0,t) \neq B_\alpha^E(\tau,t)$, yet another manifestation of the nonstationarity of fat-tailed CTRW. It should also be made clear that the time average,

$$B_\alpha^T(t) = \frac{1}{T}\int_0^T \delta C_\alpha(r,\tau)\delta C_\alpha(r,\tau + t)d\tau, \quad (9)$$

behaves differently than the previous two correlation functions, again due to the nonstationary characteristic of the system and the strong dependence on the choice of initial time ($t = 0$) and time window (T). This breaking of ergodicity is manifested when comparing the ensemble- and time-averaged MSDs as well (30). For simple diffusion, both averages coincide. However, as shown in Fig. 2, the ensemble- and time-averaged MSDs strongly differ for particles obeying Eq. 1. Thus, when analyzing time averages of single-particle tracks, care should be taken not to assume that ergodicity is fulfilled. Our definition of subdiffusion relies on the ensemble average.

Mathematical treatment of anomalous subdiffusion

We start from Fick's diffusion equation for the regular case:

$$\frac{\partial C(r,t)}{\partial t} = K\nabla^2 C(r,t), \quad (10)$$

where K is the diffusion coefficient, as in Eq. 2, and $C(r,t)$ is the concentration as a function of space and time. This equation, although ubiquitous, does not describe systems undergoing anomalous diffusion in general and subdiffusion in particular. A fractional order equation is introduced that approximates the CTRW process with fat-tailed waiting times (16):

$$\frac{\partial C_\alpha(r,t)}{\partial t} = \frac{1}{\Gamma(\alpha)}\frac{\partial}{\partial t}\int_0^t ds(t-s)^{\alpha-1}K_\alpha\nabla^2 C_\alpha(r,s), \quad (11)$$

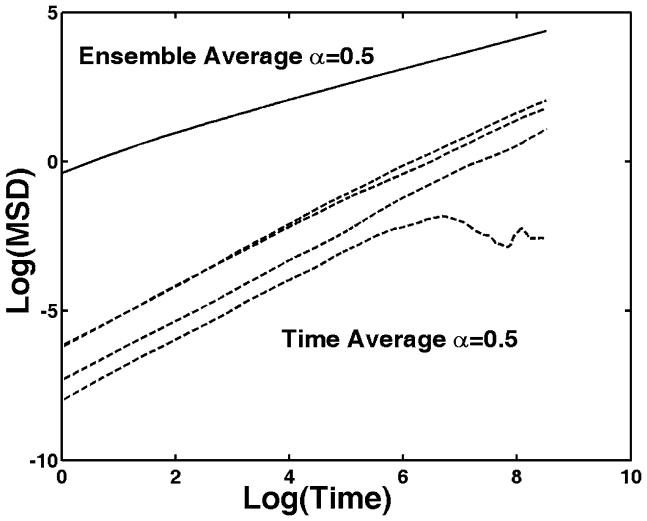

FIGURE 2 Comparison of ensemble and time averages of MSDs obtained from CTRW with $\alpha = 1/2$ plotted on log-log scales. Although the ensemble-averaged MSD has the form of Eq. 3, $\langle x^2(t)\rangle \sim t^{1/2}$, time-averaged MSDs display a distribution. The exponents of the MSDs are shown to be distributed around unity, $\langle x^2(t)\rangle \sim t$.

where $C_\alpha(r,t)$ is the concentration of the anomalous system and K_α is the anomalous diffusion coefficient, as in Eq. 3. Notice that although the CTRW process is made of independent jumps and independent waiting times, with no correlations to previous jumps or waiting times, Eq. 11 is nonlocal in time and is characterized by a long-range temporal kernel. In other words, although the motion under such a CTRW process does not explicitly include a memory (it is not Markovian, but semi-Markovian (31)), it is the nonstationary nature of the process that creates a memory kernel in Eq. 11 and is responsible for aging. This equation can be rewritten using the Riemann-Liouville operator of a noninteger order of differentiation/integration (${}_0D_t^{1-a}$, $0 < \alpha < 1$):

$$\frac{\partial C_\alpha(r,t)}{\partial t} = {}_0D_t^{1-\alpha}\left(K_\alpha\nabla^2 C_\alpha(r,t)\right). \quad (12)$$

Equations 11 and 12 reduce to the regular diffusion equation (Eq. 10) for $\alpha = 1$.

As shown in (16,32,33), one can relate the solution of the diffusion equation (Eq. 10) and that of the FDE (Eq. 11) (see Appendix):

$$C_\alpha(r,t) = \int_0^\infty dsA(s,t)\cdot C(r,s^*), \quad (13)$$

where $s^* = \frac{K_\alpha}{K}s$, $C_\alpha(r,t)$ is the solution of the FDE (Eq. 12), and $C(r,s^*)$ is the concentration of the regular system, which is the solution of Eq. 10 for the same starting and boundary conditions. The solutions are related through an integral form where $A(s,t)$, which serves as a kernel function, is the modified one-sided Levy distribution function (16). The variable s is used as an internal variable representing time, but it has the dimensions of [time$^\alpha$]. This distribution function has a series representation for the general case of any anomalous exponent α,

$$A(s,t) = \frac{1}{s}\sum_{n=0}^\infty \frac{(-1)^n}{\Gamma(1-\alpha-\alpha n)\Gamma(1+n)}\left(\frac{s}{t^\alpha}\right)^{1+n}, \quad (14)$$

and a simple functional form for some special cases of $\alpha = 1/2$ and $\alpha = 1/3$.

It is important to note that the CTRW description of anomalous diffusion is not the only model that describes anomalous diffusion. A commonly used approach is the fractional Brownian motion (FBM) (34–36), which also leads to subdiffusion. This model has infinitely long-range correlations. In particular, past increments are correlated with future increments, unlike in the CTRW model, where increments are independent. The behavior of the MSD, however, is similar to that obtained in the case of CTRW anomalous subdiffusion. Another generalization of the normal diffusion equation for the case of anomalous diffusion is the time-dependent diffusion coefficient (TDDC), which replaces the diffusion constant (13):

$$\frac{\partial C(r,t)}{\partial t} = \alpha K t^{\alpha-1}\nabla^2 C(r,t). \quad (15)$$

Being local in time, the equation does not describe the long-range temporal correlations typical of FBM, although its solution has a Gaussian-type solution that yields the same concentration as the FBM process. One should be aware that CTRW and TDDC describe different physical processes.

Fractional FCS

In FCS experiments one measures the correlation of the fluorescence fluctuations at different times. The fluorescence is defined as (5)

$$f(t) = \int d^2 r I(r) C(r,t), \quad (16)$$

where $I(r)$ is the laser beam intensity profile and $C(r,t)$ is the two-dimensional fluorophore concentration. The fluorescence fluctuations are defined by

$$\delta f(t) = \int d^2 r I(r) \delta C(r,t), \quad (17)$$

and the correlation of the fluorescence fluctuations is an average of fluctuations at two different times:

$$G(t) = \langle \delta f(\tau) \times \delta f(\tau + t) \rangle, \quad (18)$$

The average, as mentioned, can be performed in two ways, by means of a time average done on a single measurement over a long time (the usual experimental method) or using an ensemble average. In systems that manifest normal diffusion, these two averages yield the same result and such systems are known to be ergodic. The time average is written as

$$G(t) = \frac{1}{T}\int_0^T \delta f(\tau)\delta f(\tau + t) d\tau = \langle \delta f(0)\delta f(t) \rangle_T, \quad (19)$$

where $\langle\rangle_T$ indicates a time average. Using Eq. 17, we can rewrite Eq. 19 to obtain

$$G(t) = \int d^2 r \int d^2 r' I(r) I(r') \langle \delta C(r,0)\delta C(r',t) \rangle_T, \quad (20)$$

which we call the FCS curve. For a two-dimensional lateral diffusion of fluorophores in a cell membrane with a Gaussian laser beam profile, the FCS curve is given by (10,11)

$$G(t) = \frac{q^2 P_0^2 \overline{C}}{\pi(w^2 + 4Kt)}, \quad (21)$$

where $\overline{C}$ is the average concentration, q is a product of all quantum efficiencies of light absorption, emission, detection, and attenuation factors of the beam during observation, P_0 is the total laser power, and w is the radius where the laser intensity decreases to e^{-2} of its value at $r = 0$.

Let us consider the case of a system that displays subdiffusion that stems from waiting-time PDFs with no mean waiting time, modeled as a CTRW. Since here we expect aging (24,25) with time and breakdown of ergodicity, the ensemble and temporal averages do not coincide in a way which resembles the difference of averaging the MSD. We first calculate the ensemble average. If the fluorophore concentration follows Eq. 11, the correlation of concentration fluctuations (28) is

$$B_\alpha^E(r,r',\tau,t) = \langle \delta C_\alpha(r,\tau)\delta C_\alpha(r',\tau + t) \rangle. \quad (22)$$

This function depends specifically on τ and on t because of the nonstationary character of the system. As mentioned, we assume that $\tau = 0$:

$$B_\alpha^E(r,r',t) = \langle \delta C(r,0)\delta C_\alpha(r',t) \rangle. \quad (23)$$

Note that only the time evolution of fluctuation, and not the starting condition, depends on α; therefore, we have taken out the subscript α from the initial concentration fluctuation. We proceed by using Eq. 13:

$$B_\alpha^E(r,r',t) = \int_0^\infty A(s,t) \langle \delta c(r,0)\delta c(r',s) \rangle ds, \quad (24)$$

and substituting this in Eq. 20, we obtain

$$G_\alpha(t) = \int_0^\infty A(s,t) \int d^2 r \int d^2 r' I(r) I(r') \langle \delta C(r,0)\delta C(r',s^*) \rangle ds, \quad (25)$$

which can be rewritten, using Eq. 21, as

$$G_\alpha(t) = \int_0^\infty A(s,t) G(s) ds = \int_0^\infty ds A(s,t) \frac{q^2 P_0^2 \overline{C}}{\pi(w^2 + 4Ks^*)}. \quad (26)$$

Equation 26 is the main result of this study for the ensemble-averaged FCS. This result is similar to that obtained in (23) for measurements of fluorescence recovery after photobleaching.

A few points should be noted. First, in general, the starting time of FCS experiments might not correspond to the starting time of the movement of the proteins. Nevertheless, the treatment we have presented is still applicable for experimental realizations in the following cases:

1. It works when the waiting-time PDF has a power-law behavior that is truncated at large times (38). The behavior encountered for short and intermediate times is anomalously subdiffusive, whereas normal behavior is expected at large times. As the time window for the power

law is expanded, the apparent anomalous diffusion is better observed. In this case, the aging and ergodicity breaking cease to exist. We believe that the mathematical derivation presented (Eq. 26) is valid for analyzing FCS data even in a case such as this.

2. The second case raises a challenge for an experiment that one could perform, referring to Eq. 6. Lowering the temperature of a system to $< T_0$ would lead to a transition from normal to anomalous behavior. If this temperature change could be made more abrupt, the initial time of measurement would be more precise.
3. In a system manifesting such anomalous subdiffusion, the laser beam might bleach some of the nonmoving proteins. The use of an attenuated laser beam can make this problem less dramatic, but probably creates a new problem of lowering the signal/noise ratio.

Second, using the TDDC equation is problematic, as mentioned previously. If it approximates FBM, then it does not contain the correlation essential to the process. In addition, it is not clear from which time (t) one should integrate this equation when solving it. This can be related to the same aging phenomena that appear in the CTRW process.

Simulations versus calculations

We continue by calculating the FCS curve that results from the TDDC (Eq. 15). The FCS curve can be derived in a straightforward way according to the same procedure used for the derivation in the case of normal diffusion. For this case, the FCS curve has a simple functional form (8):

$$G(t) = \frac{q^2 P_0^2 \overline{C}}{\pi(w^2 + 4K_\alpha t^\alpha)}, \tag{27}$$

which differs from the normal result by introducing the time to the power of α. In addition, we calculated FCS curves as described above, using CTRW (Eq. 26) for three anomaly exponents (α), and compared them to the curves obtained from Eq. 27, where all the parameters were the same. This comparison is presented in Fig. 3.

We then checked whether the behavior of the anomalous FCS curve (as obtained from Eq. 26) has the same asymptotic behavior as Eq. 27. Fig. 4 shows a log-log of the FCS curve. A transformation to a power-law behavior is observed, which is of the same order as the anomaly order. However, the asymptotic power-law behavior appears only at extremely large times (Fig. 5).

We next check the validity of our calculations using computer simulations. We first simulated normal diffusion using a two-dimensional CTRW process. We used a grid surface of 1414×1414 over which we scattered 2×10^4 particles. At each time unit, all the particles performed a one-grid unit jump in a random direction (left, right, up, or down). We simulated a Gaussian laser beam at the center of the surface with a radius of 100 grid units. The fluorescence collected from the surface was the sum of the fluorescence of all single particles. We used the laser beam to calculate each particle's fluorescence based on its two-dimensional position. We compared the plots of the calculated FCS curve to the simulation (Fig. 6 *a*) and got excellent agreement. The initial time correlation

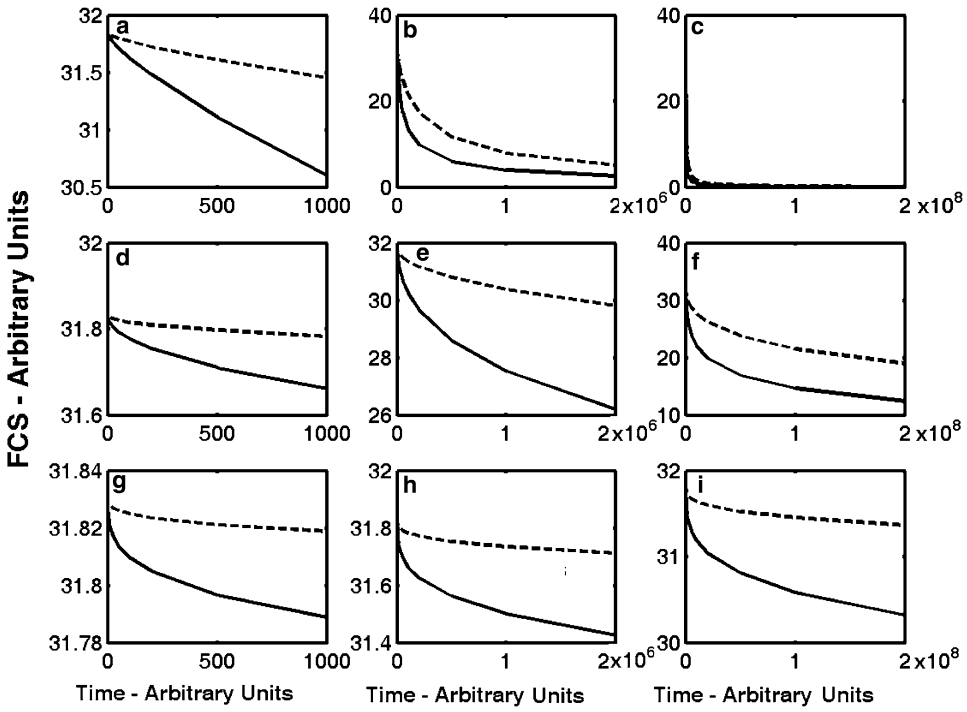

FIGURE 3 Comparison of the FDE and TDDC curves of FCS with the same parameters. In all plots, the FDE curve is plotted as a solid line and the TDDC curve is plotted as a dashed line. The lines (*top to bottom*) are for $\alpha = 0.8$ (plots *a–c*), $\alpha = 0.5$ (plots *d–f*), and $\alpha = 0.3$ (plots *g–i*). The columns are for (*left to right*) times $t = 1000$, $t = 2 \times 10^6$, and $t = 2 \times 10^8$. We observe that as α decreases, the deviation between the two curves increases. For short times, the deviation is significant, but it decreases for large times (plot *c*).

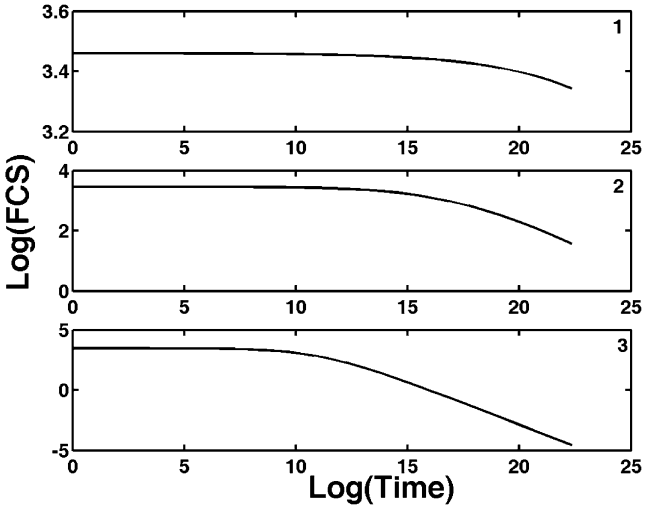

FIGURE 4 Log-log plots of the FCS curves as calculated from Eq. 26 for $\alpha = 0.3$ (plot 1), $\alpha = 0.5$ (plot 2), and $\alpha = 0.8$ (plot 3).

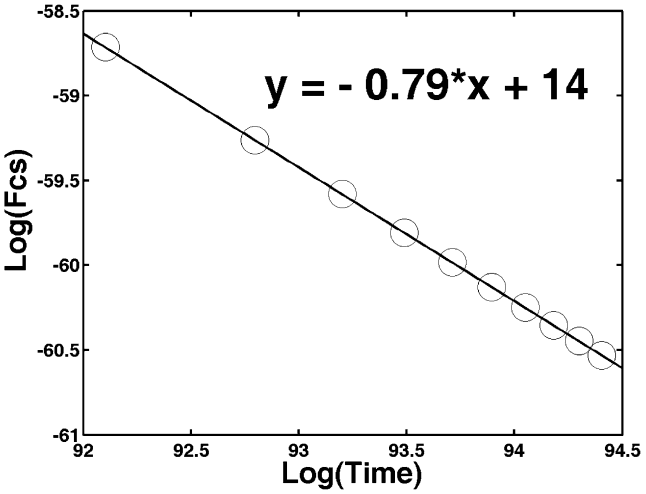

FIGURE 5 Log-log plots for extremely long times where the anomaly order is recovered. Here, the anomaly order is $\alpha = 0.8$.

$(G(0))$, according to the parameters used: $P_0 = 10000$, and $w = 100$, is

$$G(0) = \frac{P_0^2\overline{C}}{\pi w^2} = \frac{100}{\pi} = 31.8, \tag{28}$$

which is in excellent agreement with the simulation, where $G(0) = 32.2$.

We next calculated and simulated FCS curves for the case of anomalous subdiffusion. For the simulation, we used the same surface as in the case of normal diffusion. The difference was that now each particle performed a jump after a certain waiting time taken from a fat-tailed PDF. We used the algorithm in (39,40) to obtain a power-law distribution of waiting times. The proteins were ordered according to their jumping times by the heap algorithm (41). After each jump, a protein was assigned a new jumping time and put into the heap to queue.

For the calculation, we chose the simplest closed form of $A(s,t)$ which for the case of $\alpha = 1/2$ is $A(s,t) = \frac{1}{\sqrt{\pi t}}\exp(-\frac{s^2}{4t})$. For this case, Eq. 26 takes the form

$$G_\alpha(t) = \int_0^\infty ds \frac{1}{\sqrt{\pi t}} e^{-s^2/4t} \frac{q^2 P_0^2 \overline{C}}{\pi(w^2 + 4Ks)}. \tag{29}$$

Applying the definition

$$x = \frac{w^2}{8K_\alpha}, \tag{30}$$

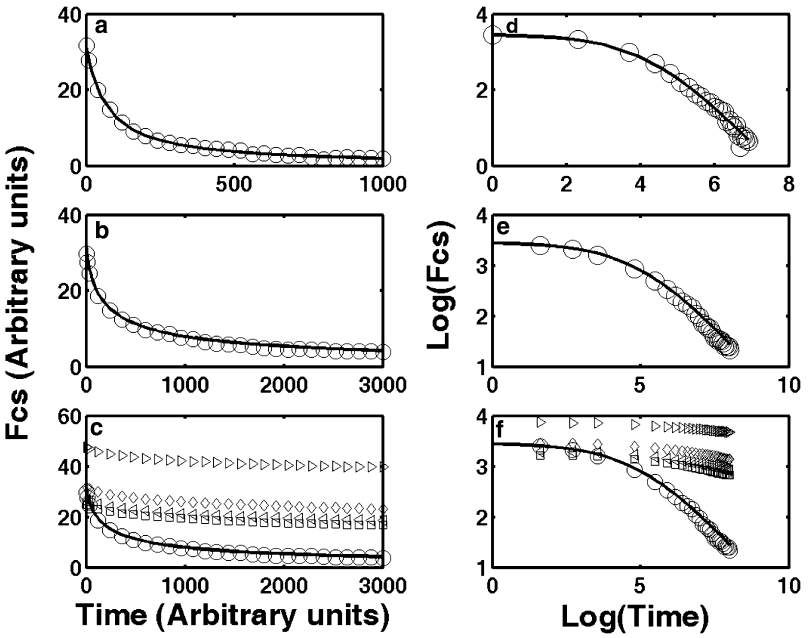

FIGURE 6 (*a*) Ensemble-averaged FCS for the case of normal diffusion. (*b*) Ensemble-averaged FCS for the case of $\alpha = 0.8$. Solid lines represent the calculation and empty circles the simulation in *a* and *b*. (*c*) Comparison of ensemble- and time-averaged FCS curves in the case of subdiffusion with $\alpha = 0.8$. Although the ensemble average follows Eq. 26, the time average displays a distribution rather than a single behavior. The time average is performed on a single realization of a system manifesting anomalous subdiffusion. As time evolves, more and more particles become immobile, and as a consequence, the overall fluorescence of the system hardly changes with time. Since the particles in each system get stuck at different locations we obtain a distribution of the fluorescence, and therefore a distribution of FCS curves. Solid lines represent the ensemble-averaged calculation, and empty circles the ensemble-averaged simulation. All other symbols correspond to time-averaged simulations of a single realization. Plots *d–f* are log-log graphs of plots *a–c*, respectively.

the integral in Eq. 29 can be calculated using Mathematica software (Wolfram Research, Champaign, IL):

$$G_\alpha(t) = \frac{e^{-x^2/t}}{8\pi^{3/2}K_\alpha\sqrt{t}}\left[\pi \mathrm{Erf}i\left[\frac{x}{\sqrt{t}}\right] - \mathrm{Cos}h\mathrm{Integral}\left[\frac{x^2}{t}\right] - \mathrm{Sin}h\mathrm{Integral}\left[\frac{x^2}{t}\right]\right], \tag{31}$$

where *Erfi*(*z*)gives the imaginary error function *erf*(*iz*)/*i* (21). The two integrals in Eq. 31 can also be found in (21). We compared this result to a computer simulation of an ensemble of particles performing a CTRW process of jumps followed by waiting times chosen from a fat-tailed distribution. The anomalous diffusion coefficient,K_α, used for the calculation is equal to the one used in the simulation and obtained good agreement (not shown). In addition, we simulated anomalous diffusion for $\alpha = 0.8$ and, using Mathematica, compared it to numerical calculations that used the series representation (Eq. 14). A comparison of the simulation and calculation shows excellent agreement between the two (Fig. 6 *b*). Fig. 6 *c* presents a comparison of ensemble and time averages. As mentioned above, systems manifesting subdiffusion are nonstationary and display aging and ergodicity breaking. Although the ensemble average can be calculated as shown above, time averages do not converge to a single function but rather are distributed. Furthermore, the time averages decay more slowly than the ensemble average, because as time progresses, particles slow their jumping rate (28), and therefore, an FCS curve, which is measured for longer times than the ensemble averages, decays more slowly. In addition, time averages depend on the time window of the measurement. This means that as the time window increases, the decay of the FCS curve slows down. Another point to mention is that the power-law asymptotic decay of the FCS function is reached for longer times only compared to the decay presented in Fig. 6 *b*.

We then fitted Eq. 27 to our calculated CTRW curve for $\alpha = 0.5$ (shown in Fig. 7). We made two kinds of fits: the first was a one-parameter fit of the diffusion coefficient, K_α, only (where α was fixed, assumed known) and the second a two-parameter fit to the diffusion coefficient and to α. Fitting both α and the diffusion coefficient, we obtained a 16% error for α and a much larger deviation for the diffusion coefficient (about a factor of 3). This two-parameter fit agrees better with the CTRW curve, as can be seen in Fig. 7 for both short times (Fig. 7 *a* and a log-log plot, Fig. 7 *c*) and long times (Fig. 7 *b* and a log-log plot, Fig. 7 *d*). When performing a one-parameter fit of the diffusion coefficient (with $\alpha = 0.5$ is assumed), we obtained a better value of the diffusion coefficient, with $<20\%$ error.

We have revisited the theory of FCS for particles, performing CTRW/FDE with fat-tailed waiting-time PDFs. We compared the CTRW results to the more commonly used TDDC equation and highlighted effects of aging and ergodicity breaking, which should be amenable to experimental tests.

APPENDIX: RELATIONSHIP BETWEEN SOLUTIONS OF FRACTIONAL AND REGULAR DIFFUSION EQUATIONS (SUBORDINATION)

The appendix relies on derivations in references (16,32,42). We show a relationship between the solutions of fractional and regular diffusion equations that is also known as subordination. This relationship is valid for the case where both fractional and regular PDEs have the same initial and boundary conditions:

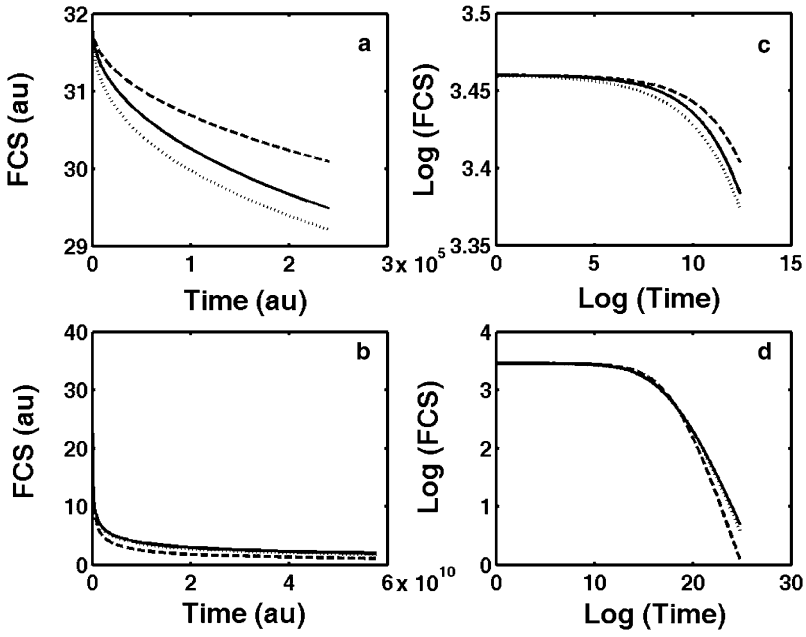

FIGURE 7 Comparison of CTRW/FDE and TDDC FCS curves for (*a*) short times and (*b*) long times, where solid lines represent the FDE calculated curve, dotted lines the two-parameter TDDC fit, and dashed lines the one-parameter TDDC fit. Data are given in arbitrary units (au). (*c* and *d*) Same data as in *a* and *b*, respectively, on a log-log scale.

$$C_\alpha(x,t) = \int_0^\infty dsA(s,t)C(x,s^*), \quad \text{(A1)}$$

where $s^* = \frac{K_\alpha}{K}s$, K_α and K are the anomalous and regular diffusion coefficients, respectively, $C_\alpha(x,t)$ is the solution of the fractional differential equation, and $C(x,t)$ is the solution of the regular diffusion equation (s represents an internal time variable). $A(s,t)$, which serves as a kernel function, is the modified one-sided Levy distribution (16,31). The subordination accounts for the time cost of simple random-walk steps due to waiting times and it generally offers a translation of the number of steps into time (22). We turn to prove the identity of Eq. A1. We start by writing the fractional differential equation, Eq. 11:

$$\begin{aligned} C_\alpha(x,t) - C_\alpha(x,0) &= {}_0D_t^{-\alpha}K_\alpha\frac{\partial^2}{\partial x^2}C_\alpha(x,t) \\ &= K_\alpha\int_0^t \kappa(t-t')\frac{\partial^2}{\partial x^2}C_\alpha(x,t')dt'. \end{aligned} \quad \text{(A2)}$$

Laplace transforming leads to (31):

$$C_\alpha(x,u) - C_\alpha(x,0)/u = K_\alpha\kappa(u)\frac{\partial^2}{\partial x^2}C_\alpha(x,u). \quad \text{(A3)}$$

In the same way, we transform Eq. A1 to Laplace space to reach an equation for the regular concentration $C(x,t)$:

$$\begin{aligned} C_\alpha(x,u) &= \int_0^\infty \exp(-ut)dt\int_0^\infty dsA(s,t)C(x,s^*) \\ &= \int_0^\infty dsA(s,u)C(x,s^*). \end{aligned} \quad \text{(A4)}$$

We next present $A(s,u)$ as

$$A(s,u) = \frac{1}{u\kappa(u)}\exp\left[-s\frac{1}{\kappa(u)}\right], \quad \text{(A5)}$$

where $\kappa(u)$ is the same function that appears in Eq. A3. Here, $A(s,u)$ is the Laplace transform of Eq. 14, with $\kappa(u)\sim u^{-\alpha}$. Substituting this into Eq. A4 yields

$$C_\alpha(x,u) = \int_0^\infty dsC(x,s^*)\frac{1}{u\kappa(u)}\exp\left[-s\frac{1}{\kappa(u)}\right], \quad \text{(A6)}$$

which is actually a Laplace transform for $C(x,s)$, so that

$$C_\alpha(x,u) = \frac{K}{K_\alpha u\kappa(u)}C\left(x,\frac{K}{K_\alpha\kappa(u)}\right). \quad \text{(A7)}$$

We rewrite Eq. A3 using Eq. A7:

$$\frac{K}{K_\alpha\kappa(u)}C\left(x,\frac{K}{K_\alpha\kappa(u)}\right) - C_\alpha(x,0) = K\frac{\partial^2}{\partial x^2}C\left(x,\frac{K}{K_\alpha\kappa(u)}\right). \quad \text{(A8)}$$

The requirement states that the initial conditions are the same for both the regular and anomalous cases: $C_\alpha(x,0) = C(x,0)$. We change variables,

$$z = \frac{K}{K_\alpha\kappa(u)}, \quad \text{(A9)}$$

and finally obtain

$$zC(x,z) - C(x,0) = K\frac{\partial^2}{\partial x^2}C(x,z), \quad \text{(A10)}$$

which is just the Laplace transform of the regular diffusion equation. We have shown that the subordination relationship (Eq. A1) is fulfilled when one substitutes Eq. A5. Namely, there exists an integral relation between the fractional and regular solutions of the corresponding diffusion equations.

REFERENCES

1. Zhang, F., G. M. Lee, and K. Jacobson. 1993. Protein lateral mobility as a reflection of membrane microstructure. *Bioessays*. 15:579–588.
2. Henis, Y. I., B. Rotbalt, and Y. Kloog. 2006. Frap beam-size analysis to measure palmitoylation-dependent membrane association dynamics and microdomain partitioning of Ras proteins. *Methods*. 40:183–190.
3. Niv, H., O. Gutman, Y. Kloog, and Y. I. Henis. 2002. Activated K-Ras and H-Ras display different interactions with saturable nonraft sites at the surface of live cells. *J. Cell Biol.* 157:865–872.
4. Ryan, T. A., S. J. Smith, and H. Reuter. 1996. The timing of synaptic vesicle endocytosis. *Proc. Natl. Acad. Sci. USA*. 93:5567–5571.
5. Axelrod, D., D. E. Koppel, J. Schlessinger, E. Elson, and W. W. Webb. 1976. Mobility measurement by analysis of fluorescence photobleaching recovery kinetics. *Biophys. J.* 16:1055–1069.
6. Ghosh, R. N., and W. W. Webb. 1994. Automated detection and tracking of individual and clustered cell-surface low-density-lipoprotein receptor molecules. *Biophys. J.* 66:1301–1318.
7. Kusumi, A., Y. Sako, and M. Yamamoto. 1993. Confined lateral diffusion of membrane receptors as studied by single-particle tracking (nanovid microscopy): effects of calcium-induced differentiation in cultured epithelial cells. *Biophys. J.* 65:2021–2040.
8. Weiss, M., H. Hashimoto, and T. Nilsson. 2003. Anomalous protein diffusion in living cells as seen by fluorescence correlation spectroscopy. *Biophys. J.* 84:4043–4052.
9. Weiss, M., M. Elsner, F. Kartberg, and T. Nilsson. 2004. Anomalous subdiffusion is a measure for cytoplasmic crowding in living cells. *Biophys. J.* 87:3518–3524.
10. Elson, E. L., and D. Magde. 1974. Fluorescence correlation spectroscopy. 1. Conceptual basis and theory. *Biopolymers*. 13:1–27.
11. Elson, E. L. 1985. Fluorescence correlation spectroscopy and photobleaching recovery. *Annu. Rev. Phys. Chem.* 36:379–406.
12. Risken, H. 1989. The Fokker-Planck Equation, 2nd ed. Springer-Verlag, Berlin.
13. Saxton, M. J. 2001. Anomalous subdiffusion in fluorescence photobleaching recovery: a Monte Carlo study. *Biophys. J.* 81:2226–2240.
14. Saxton, M. J. 2007. A biological interpretation of transient anomalous subdiffusion. I. Qualitative model. *Biophys. J.* 92:1178–1191.
15. Montroll, E. W., and G. H. Weiss. 1969. Random walks on lattices II. *J. Math. Phys.* 6:167–181.
16. Metzler, R., and J. Klafter. 2000. The random walk's guide to anomalous diffusion: a fractional dynamics approach. *Phys. Rep.* 339:1–77.
17. Bouchaud, J. P., and A. Georges. 1990. Anomalous diffusion in disordered media - statistical mechanisms, models and physical applications. *Phys. Rep.* 195:127–293.
18. Barkai, E., R. Metzler, and J. Klafter. 2000. From continuous time random walks to the fractional Fokker-Planck equation. *Phys. Rev. E Stat. Phys. Plasmas Fluids Relat. Interdiscip. Topics*. 61:132–138.
19. Scher, H., and E. W. Montroll. 1975. Anomalous transit-time dispersion in amorphous solids. *Phys. Rev. B*. 12:2455–2477.
20. Nagle, J. F. 1992. Long tail kinetics in biophysics? Biophys. J. 63:366–370.

21. Abramowitz, M., and I. A. Stegun. 1972. Handbook of Mathematical Functions. Dover, New York.

22. Blumen, A., J. Klafter, and G. Zumofen. 1986. Reaction in disordered media, modelled by fractals. *In* Fractals in Physics. L. Pietronero and E. Tosatti, editors. North Holland, Amsterdam. 399–408.

23. Lubelski, A., and J. Klafter. 2008. Fluorescence recovery after photobleaching (FRAP): The case of anomalous diffusion. *Biophys. J.* 94:4646–4653.

24. Barkai, E. 2003. Aging in subdiffusion generated by a deterministic dynamical system. *Phys. Rev. Let.* 90, 104101-1–104101-4.

25. Barkai, E., and Y. C. Cheng. 2003. Aging continuous time random walk. *J. Chem. Phys.* 118:6167–6178.

26. Margolin, G., and E. Barkai. 2005. Nonergodicity of blinking nanocrystals and other Levy-walk processes. *Phys Rev. Let.* 94:080601.

27. Barkai, E., and G. Margolin. 2004. Aging, non-ergodicity, and levy statistics for blinking nanocrystals. *Isr. J. Chem.* 44:353–362.

28. Lubelski, A., and J. Klafter. 2008. Temporal correlation function of concentration fluctuations: an anomalous case. *J. Phys. Chem. B.* 112: 12740–12747.

29. Sokolov, I. M., A. Blumen, and J. Klafter. 2001. Linear response in complex systems: CTRW and the fractional Fokker-Planck equations. *Physica A.* 302:268–278.

30. Lubelski, A., I. M. Sokolov, and J. Klafter. 2008. Nonergodicity mimics inhomogeneity in single particle tracking. *Phys. Rev. Lett.* 100: 250602.

31. Feller, W. 1968. An Introduction to Probability Theory and its Applications, Vol. 2, 3rd ed. Wiley, New York.

32. Sokolov, I. M. 2002. Solutions of a class of non-Markovian Fokker-Planck equations. *Phys. Rev. E Stat. Nonlin. Soft Matter Phys.* 66:041101.

33. Metzler, R., and J. Klafter. 2003. When translocation dynamics becomes anomalous. *Biophys. J.* 85:2776–2779.

34. Lutz, E. 2001. Fractional Langevin equation. *Phys. Rev. E.* 64, 051106-1–051106-4.

35. Mandelbrot, B. B., and J. W. Van Ness. 1968. Fractional Brownian motion, fractals noise and applications. *SIAM Rev.* 10:422–437.

36. Feder, J. 1998. Fractals. Plenum Press, New York.

37. Reference deleted in proof.

38. Saichev, A. I., and G. G. Utkin. 2004. Random walks with intermediate anomalous-diffusion asymptotics. *J. Exp. Theor. Phys.* 99:443–448.

39. Weron, R. 1996. On the Chambers-Mallows-Stuck method for simulating skewed stable random variables. *Stat. Probab. Lett.* 28:165–171.

40. Chambers, J. M., C. L. Mallows, and B. W. Stuck. 1976. Method for simulating stable random-variables. *J. Am. Stat. Assoc.* 71:340–344.

41. Cormen, T. H., E. L. Charles, and R. L. Rivest. 1990. Introduction to Algorithm. MIT Press, Cambridge, MA.

42. Metzler, R., E. Barkai, and J. Klafter. 1999. Anomalous diffusion and relaxation close to thermal equilibrium: a fractional Fokker-Planck equation approach. *Phys. Rev. Lett.* 82:3563.